BUILD SIMUL (2010) 3: 205 – 214
DOI 10.1007/s12273-010-0004-5

CFD modelling of the effect of fire source geometry and location on smoke flow multiplicity

Jian Gong (✉), Yuguo Li

Department of Mechanical Engineering, The University of Hong Kong, Pokfulam, Hong Kong, China

Abstract

Understanding solution multiplicity of smoke flow at the same building configuration and ambient conditions is important for managing smoke flows and human evacuation in buildings. One of the known examples with solution multiplicity is in a simple single-compartment building on fire under an opposing wind. The occurrence of multiple solutions of smoke flow is induced by competing wind and thermal buoyancy forces. Under a given and moderate wind, the critical buoyancy flux ratio for the existence of smoke flow multiplicity, which is a ratio between defined parameters representing buoyancy force and wind pressure, is related to building height and opening area, as shown using a zone model. Computational fluid dynamics (CFD) simulations were used here to evaluate whether the behaviour of smoke flow multiplicity was affected by the geometry and location of the fire source(s). Our simulation results were in good agreement with previous macroscopic analysis results. A floor fire source can produce the largest smoke flow rate in the buoyancy-dominated flow regime among the tested cases while two corner sources can produce the smallest smoke flow rate. A floor source had a relatively large smoke flow rate in the wind-dominated flow regime while a point source had relatively small smoke flow rate. Moreover, a larger critical buoyancy flux ratio and a larger range of fire power in which smoke flow multiplicity existed were found for a floor fire source than for other sources. Switching of smoke flow solutions in building fires was found to depend on the initial conditions and the magnitude of flow perturbations.

Keywords

smoke flow,
CFD simulation,
opposing wind,
fire source,
buoyancy flux ratio,
solution multiplicity

Article History

Received: 23 March 2010
Revised: 24 May 2010
Accepted: 26 May 2010

1 Introduction

Smoke contains airborne solid, liquid particles, gases of combustion products, and a large amount of entrained air (NFPA 2009). It can threaten the life of occupants and properties during and after building fire. Smoke can flow from the fire source to other locations under one or combined driving forces. The undesirable and/or dangerous smoke flow patterns can be avoided, or the occupants in the possibly risky spaces may be evacuated immediately and safely, only if the smoke flow behaviour can be understood. An interesting and complex smoke flow phenomenon is the solution multiplicity, i.e., the multiple solutions of smoke flow can exist at the same building configuration and ambient conditions (Nitta 1999, 2001; Gong and Li 2008). Multiple solutions refer to multiple smoke flow directions, smoke flow rates, and smoke temperatures at the same boundary conditions. Different initial conditions such as temperature and smoke flow velocity can lead to different smoke flow patterns, which may switch to one another when there are sufficient perturbations of the driving force of flows. Among the multiple solutions, some are perhaps relatively safe while the others are relatively unsafe for occupants and properties. This may be important for managing smoke flows and human evacuation in buildings.

The existence of airflow multiplicity in closely related flow phenomenon, i.e., the natural ventilation of buildings (Li and Delsante 2001; Li et al. 2001; Heiselberg et al. 2004; Li et al. 2006; Linden 1999; Hunt and Linden 2004; Yuan and Glicksman 2007, 2008; Lishman and Woods 2006, 2009a, 2009b; Flynn and Caulfield 2009), is well documented. However, studies on smoke flow multiplicity are rare. In

E-mail: gongjian82@gmail.com

our recent analysis, a simple single-compartment building with two small openings on fire was considered under an opposing wind (Gong and Li 2008). Wind has a pronounced effect on smoke flow, which can exert pressure difference between windward and leeward side of a building (Klote and Milke 1992). This simple configuration is known to give two stable solutions of smoke flow with the same boundary conditions, shown in Fig. 1. The solution multiplicity is induced by competing buoyancy and wind forces. Figure 1(a) shows an upward smoke flow dominated by buoyancy force with two layers, which is thought to be relatively safe for human evacuation due to the existence of a clear lower layer. Figure 1(b) shows a downward smoke flow dominated by wind force with a fully mixed smoke flow, which is considered to be relatively unsafe as smoke spreads in the entire building.

The buoyancy force arises from the reduced density in the smoke and the smoke is formed by the fire plume, which depends on the geometry and location of fire source. Hence, the fire geometry and location can vary smoke temperature and smoke interface in a practical circumstance, such as wall fires or corner fires. Morton et al. (1956) considered the point source plume, while others considered line source and vertically distributed source (Linden et al. 1990) and floor source (Gladstone and Woods 2001). A number of different point plume models exist (Heskestad 1986; Zukoski et al. 1980; McCaffrey 1979). The plume equation from line sources was experimentally and theoretical investigated by Lee and Emmons (1961) as well as Yuan and Cox (1996). The mirror model was proposed by Zukoski (1995) to analyze the fire plume near walls or at a corner. Poreh and Garrad (2000) conducted an experimental study of a fire close to a wall and a corner, and different plume models were studied.

We used a macroscopic smoke flow zone model to demonstrate the existence of multiple smoke flow solutions (Gong and Li 2008) in a simple building as shown in Fig. 1. In this paper, we proceed to consider the critical buoyancy flux ratio when there is a flow switching from the wind-dominated to the buoyancy-dominated flow as buoyancy force increases under a fixed and moderate opposing wind using a zone model. Six different geometries and locations of fire source are analyzed here using computational fluid dynamics (CFD) simulations. The CFD results are compared with those of the macroscopic flow analysis. The effect of initial conditions and perturbations is also discussed.

2 Critical buoyancy flux ratio

The existence of a wind-dominated flow depends on the size of fire power. If the fire power is relatively small, a wind-dominated flow exists; but if the fire power is sufficiently large, the flow is buoyancy-dominated flow. In the smoke flow multiplicity phenomenon, the turning point (i.e., Point 2 in Fig. 4) from a wind-dominated flow to a buoyancy-dominated flow as the buoyancy force increases is of special interest as it represents the condition at which a major flow pattern switch occurs. We define the buoyancy flux ratio under a fixed opposing wind in the form of $\dot{m}_Q / \dot{m}_W$ at this turning point as the critical buoyancy flux ratio. The critical buoyancy flux ratio is chosen in this paper as a parameter for comparing different test cases.

We attempt to derive an analytical expression of the critical buoyancy flux ratio in the following. As the critical buoyancy flux ratio is the point at which a wind-dominated flow switches to a buoyancy-dominated flow, we approach the analysis from the wind-dominated flow equations as no solution exists beyond the critical buoyancy flux ratio. The following assumptions are made. All walls are adiabatic; the flow through the two small openings is unidirectional; the vertical distance between the two openings is the building height; the interior space smoke is fully mixed; and no thermal radiation is considered. In this situation, the ambient air enters through the top opening, mixing with the smoke in

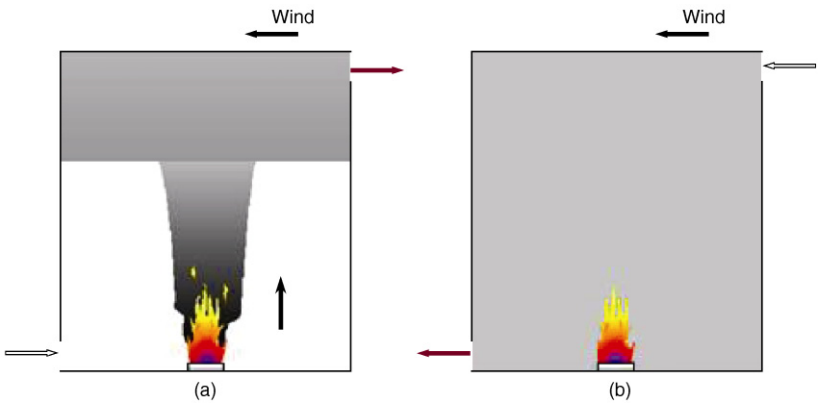

Fig. 1 Two smoke flow solutions under an opposing wind: (a) a buoyancy-dominated flow solution with an upward smoke flow and two layers; (b) a wind-dominated flow solution with a downward smoke flow and the building is fully mixed with smoke (Gong and Li 2008)

the room, and the smoke leaves the room through the bottom opening, as seen in Fig. 1(b). The governing equations are as follows:

$$\frac{\mathrm{d}(\rho_s A_c H)}{\mathrm{d}t} = \dot{m}_t - \dot{m}_b \tag{1}$$

$$c_p \frac{\mathrm{d}(\rho_s A_c H T_s)}{\mathrm{d}t} = Q_c + c_p \dot{m}_t T_0 - c_p \dot{m}_b T_s \tag{2}$$

$$\Delta P_w - (\rho_0 - \rho_s) g H = \frac{\dot{m}_b^2}{(C_d A)^2 2\rho_s} + \frac{\dot{m}_t^2}{(C_d A)^2 2\rho_0} \tag{3}$$

Equation (1) represents the mass balance in the building, while Eq. (2) represents the energy balance. Equation (3) is a pressure loop equation as there is only one pressure loop for the configuration being considered. T_s is the smoke temperature, T_0 the ambient air temperature, ρ_s the smoke density, ρ_0 the ambient air density, A_c the floor area and H the building height; ΔP_w the wind pressure between two openings; $\dot{m}_t$ and $\dot{m}_b$ the mass flow rates through the top and bottom openings, respectively (at the steady state $\dot{m}_t = \dot{m}_b$ and it is denoted as $\dot{m}$); Q_c the convective heat release rate of the fire; c_p the specific heat capacity of air; C_d discharge coefficient; A the opening area of one opening (the two openings are assumed to have the same area); g the acceleration of gravity; and t the time. In addition, the equation of state $\rho_0 T_0 = \rho_s T_s$ is used as the indoor pressure variation is relatively small compared to the ambient pressure.

Here several parameters are defined to facilitate our analysis:

$$\dot{m}_Q = Q_c / c_p T_0 \tag{4}$$

$$\dot{m}_W = (C_d A^*)\sqrt{2\rho_0 \Delta P_w} \tag{5}$$

$$\dot{m}_Z = (C_d A^*)\sqrt{2\rho_0^2 g H} \tag{6}$$

where $C_d A^* = \dfrac{(C_d A)(C_d A)}{\sqrt{(C_d A)^2 + (C_d A)^2}} = \dfrac{C_d A}{\sqrt{2}}$.

The three defined parameters $\dot{m}_Q$, $\dot{m}_W$ and $\dot{m}_Z$ have the same unit as the mass flow rate (kg/s). $\dot{m}_Z$ is related to the building height and opening area, $\dot{m}_Q$ is related to fire power, which is relevant to buoyancy force and $\dot{m}_W$ is related to wind pressure. The ratio ($\dot{m}_Q / \dot{m}_W$) between buoyancy force parameter $\dot{m}_Q$ and the wind-related parameter $\dot{m}_W$ at the turning point (i.e., Point 2 in Fig. 4) is of our interest here.

The effect of buoyancy force under a fixed wind force can be analyzed by means of simplification of Eqs. (1) – (3) into a non-dimensional ordinary differential equation:

$$f(T^*) = \frac{\mathrm{d}T^*}{\mathrm{d}\tau} = \frac{T^{*3/2}(1-T^*)}{1+T^*} \cdot \sqrt{2(1+T^*) - 2\frac{T^{*2}-1}{T^*}\left(\frac{\dot{m}_Z}{\dot{m}_W}\right)^2 - \left(\frac{\dot{m}_Q}{\dot{m}_W}\right)^2} + \frac{2T^{*2}}{1+T^*}\frac{\dot{m}_Q}{\dot{m}_W} \tag{7}$$

where $\tau = t\dot{m}_W / M$ is a non-dimensional time, $M = \rho_0 A_c H$ (has a unit of mass), and $T^* = T_s / T_0$ is a non-dimensional temperature.

The steady state equation of $\mathrm{d}T^*/\mathrm{d}\tau = 0$ can be obtained

$$T^*(T^*+1)\left(\frac{\dot{m}_Q}{\dot{m}_W}\right)^2 + 2(T^*-1)^3\left(\frac{\dot{m}_Z}{\dot{m}_W}\right)^2 - 2T^*(T^*-1)^2 = 0 \tag{8}$$

The critical ratio ($\dot{m}_Q / \dot{m}_W$) occurs when Eq. (8) has one solution, and beyond this point, Eq. (8) has no solution. We choose a group of typical values, $H = 3$ m, $A = 0.2$ m^2, $T_0 = 300$ K, $c_p = 1006.7$ J/(kg·K), $\rho_0 = 1.225$ kg/m^3, $C_d = 0.6$, $\Delta P_w = 16$ Pa, then a value of $\dot{m}_Z / \dot{m}_W = 1.5$ is obtained, and the relationship between $\mathrm{d}T^*/\mathrm{d}\tau$ and $T^* = T_s/T_0$ is shown in Fig. 2 for different $\dot{m}_Q / \dot{m}_W$ values. We can see that the equation has zero (when $\dot{m}_Q / \dot{m}_W = 0.25$), one (when $\dot{m}_Q / \dot{m}_W \approx 0.224$) or two (when $\dot{m}_Q / \dot{m}_W = 0.18$) solutions at the steady state ($\mathrm{d}T^*/\mathrm{d}\tau = 0$). The stability of the possible two solutions can be evaluated by the slope sign at the solution (Strogatz 1994).

Equation (8) is used to plot a graph of $1/T^*$ versus $\dot{m}_Q / \dot{m}_W$ for different $\dot{m}_Z / \dot{m}_W$ values in Fig. 3. The critical $\dot{m}_Q / \dot{m}_W$ value is found when there is one solution of T^* in Eq. (8) as $\dot{m}_Q / \dot{m}_W$ value increases. The larger the $\dot{m}_Z / \dot{m}_W$

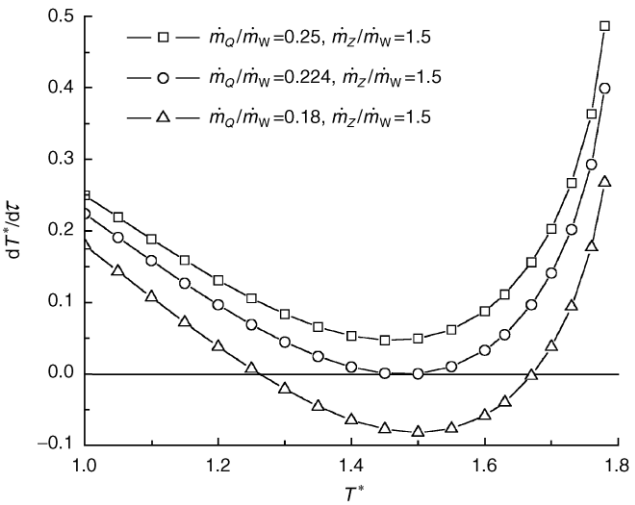

Fig. 2 Curves of $f(T^*)$ versus T^* for different $\dot{m}_Q / \dot{m}_W$ values when $\dot{m}_Z / \dot{m}_W = 1.5$

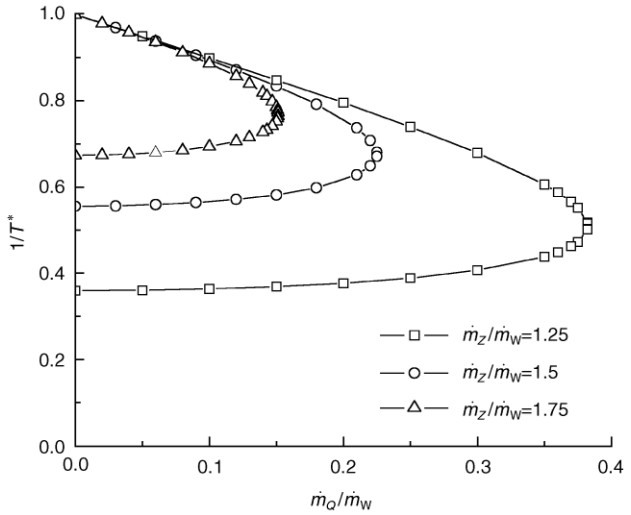

Fig. 3 Curves of $1/T^*$ versus $\dot{m}_Q/\dot{m}_W$ for different $\dot{m}_Z/\dot{m}_W$ values

value, the smaller the critical $\dot{m}_Q/\dot{m}_W$ value is. When Eq. (8) has one solution, $\mathrm{d}(\dot{m}_Q/\dot{m}_W)/\mathrm{d}T^* = 0$. On the basis of $\mathrm{d}(\dot{m}_Q/\dot{m}_W)/\mathrm{d}T^* = 0$, the critical $\dot{m}_Q/\dot{m}_W$ value as a function of a given $\dot{m}_Z/\dot{m}_W$ value can be obtained after some manipulation:

$$T_{cri}^{*2}(T_{cri}^{*}+3) = \left(\frac{\dot{m}_Z}{\dot{m}_W}\right)^2 (T_{cri}^{*}-1)(T_{cri}^{*2}+4T_{cri}^{*}+1) \tag{9}$$

here T_{cri}^{*} is the critical non-dimensional temperature. By substituting the solution of T_{cri}^{*} from Eq. (9) to Eq. (8), the critical $\dot{m}_Q/\dot{m}_W$ value, namely the critical buoyancy flux ratio, where the wind-dominated flow solution switches to the buoyancy-dominated flow solution, can be obtained and the value is denoted as $(\dot{m}_Q/\dot{m}_W)_{cri}$. The analytical solution of the critical $\dot{m}_Q/\dot{m}_W$ value is a root of cubic equation and is lengthy, so it is not shown here. The condition of $0 < \dot{m}_Q/\dot{m}_W \leqslant (\dot{m}_Q/\dot{m}_W)_{cri}$ gives the range of buoyancy force in which the multiple solutions of smoke flow exist under a fixed and moderate wind force. In the following CFD analysis, the critical $\dot{m}_Q/\dot{m}_W$ values of different cases are predicted.

3 CFD modeling

A three dimensional CFD model was used to simulate smoke flow in the simple building under an opposing wind by means of the commercial software Fluent 6.3.26. Only half of the building was simulated by making use of the symmetry boundary condition. The entire size of building and fire source is described below. A simple two-way simulation approach (Albensoeder et al. 2001) was employed to consider the effect of different initial conditions. The simulation results were compared with the macroscopic flow analysis (Gong and Li 2008).

In a previous macroscopic analysis study (Gong and Li 2008), the following variable $\dot{m}_A$ was defined when analyzing the buoyancy-dominated flow regime.

$$\dot{m}_A = \left[2(C_d A^*)^2 \rho_0^{8/5} g^{4/5} \frac{1}{E^{3/5}}\right]^{5/8} \tag{10}$$

where $E = 0.196$ is a constant (Heskestad 1986), the parameter $\dot{m}_A$ was related to the effect of opening area of building. We considered the group of typical values above and the approximate values of $\dot{m}_A/\dot{m}_W = 1.1$ and $\dot{m}_Z/\dot{m}_W = 1.5$ are obtained (Gong and Li 2008). Using Eqs. (8) – (9), the critical buoyancy flux ratio was found to be $(\dot{m}_Q/\dot{m}_W)_{cri} \approx 0.2241$.

In CFD simulations, the same size of two small openings of the half building was firstly set with 1 m wide and 0.2 m high. The height of the openings was sufficiently small to satisfy the unidirectional flow assumption as in the macroscopic flow analysis. To satisfy $\dot{m}_A/\dot{m}_W = 1.1$ and $\dot{m}_Z/\dot{m}_W = 1.5$, the height of the building can be determined to be 3 m. The half building was also chosen to be 2 m long and 1 m wide. The wall thickness is 0.1 m.

The computational domain for our CFD simulations was $21.3H$ long, $5.3H$ wide and $6.3H$ high, where H is the building height $H = 3$ m. The computational domain only covers half of the physical domain. One side of the computational domain coincides with the symmetry plane of the building. Hence the width of the physical domain is $2 \times 5.3H = 10.6H$. The building penetrates only $0.3H$ into the computational domain. The building was situated at $5.3H$ downstream of the flow inlet, and the lateral extension was $5H$, vertical extension was $5.3H$.

Only the steady state simulations were carried out and the thermal radiation was not considered to accord with macroscopic analysis. A RNG k-ε turbulence model was used and all the smoke flow properties were set to be constant except that the ideal gas equation was used to calculate the density variation of gas due to high temperature. The enhanced wall treatment was used for the near-wall treatment. The SIMPLE algorithm was used for the pressure and velocity coupling. The second-order upwind scheme was employed in discretizing the convection terms. The non-slip condition and the zero heat flux were used at the solid surfaces. Since the flow is compressible, the mass flow inlet boundary condition was applied at the wind inlet boundary of the computational domain, and the pressure outlet boundary condition at the outflow boundary. Symmetry boundary condition was applied in the lateral and vertical boundaries. No boundary conditions are needed at the two openings of the building. Two meshes with 0.5 million and 0.75 million grid points were used with finer grids close to the building

walls. The mass flow rate $\dot{m}$ through the openings was used as the solution indicator in our simulations. The two meshes were shown to give nearly the same results.

This two-way simulation procedure is shown in Fig. 4. A CFD simulation without fire was first performed to satisfy the prescribed ambient wind condition $\dot{m}_W$ value, so the wind speed was determined to be 5.3 m/s. The mass flow can then be obtained by multiplying wind speed with the density of ambient air $\rho_0 = 1.225$ kg/m^3. Under the given opposing wind, the fire power was increased from zero (Point 1) step by step (initial step size is 16 kW) until the wind-dominated flow solution switched to the buoyancy-dominated flow solution at Point 2, then we continued to increase the fire power to Point 4, which lied in the buoyancy-dominated flow regime. After that, we decreased the fire power step by step, and the buoyancy-dominated flow solution was not found to switch to the wind-dominated flow solution at Point 3. Instead, it was kept to be buoyancy-dominated flow regime with a reduced mass flow rate, and it switched to wind-dominated flow regime at Point 5. The unstable branch cannot be obtained in our CFD simulations. Here the buoyancy-dominated flow regime was denoted as positive while the wind-dominated flow regime as negative. We will compare the macroscopic theoretical analysis (Gong and Li 2008) in Fig. 4 with CFD simulations below in Fig. 8.

Six different geometries and locations of fire source were considered; see Fig. 5. All fire sources were 0.2 m high.

- Point source. The half fire source was 0.2 m long and 0.1 m wide, located at the middle of the building at the floor level; see Fig. 5(a). It is not exactly a point source, but with a relatively small fire size.
- Floor source. The half fire source was 2 m long and 1 m wide, located at the floor level; see Fig. 5(b).
- Line source Ⅰ. The half fire source was 0.2 m long and 1m wide, located in the middle of the floor, and it was perpendicular to the symmetry plane; see Fig. 5(c).

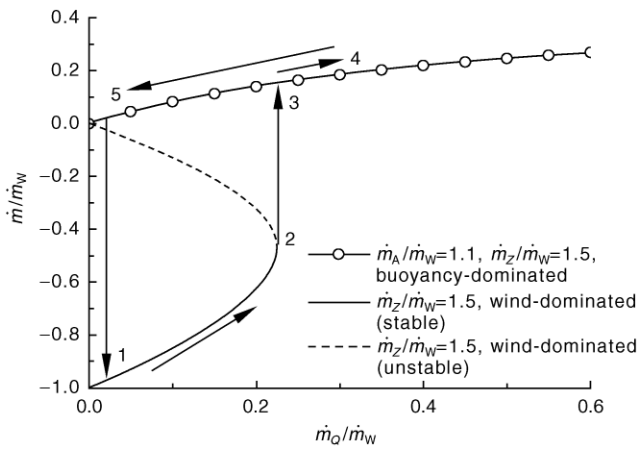

Fig. 4 The two-way simulation procedure used in CFD simulations

- Line source Ⅱ. The half fire source was 2 m long and 0.1 m wide, and it was parallel to the symmetry plane; see Fig. 5(d).
- Wall source. The half fire source was 0.2 m long and 0.1 m wide, located at the floor level, adjacent to the centre of one of the side walls; see Fig. 5(e).
- Corner sources. Two point sources located at two corners on the floor as displayed in Fig. 5(f) and the size of each source was 0.2 m long and 0.1 m wide.

4 Results

4.1 Predicted smoke flow patterns

We first present typical predicted smoke flow patterns as shown by the isotherm contours. We choose to present the situation when two solutions exist ($\dot{m}_Q/\dot{m}_W \approx 0.0982$, corresponding to a fire power of 32 kW). The buoyancy-dominated flow solutions are shown in Fig. 6 and the wind-dominated flow solutions are shown in Fig. 7 on the cut planes shown in Fig. 5.

For the buoyancy-dominated solutions, the overall smoke flow direction is upwards. The level of thermal stratification in the building differs for different fire sources. Concentrated fire sources such as point source, wall source and corner sources produce thermally stratified solutions, while the distributed sources such as floor source and line sources produce rather uniform smoke temperature distribution in the building.

For the wind-dominated flow solutions, the stronger wind overcomes the buoyancy force and flows in through the top opening. The wind flow induces a strong mixing of smoke in the building then flows out through the bottom opening. In general, the flow is rather uniform within the building. In Fig. 7, the value difference among isotherms is small. The indoor temperature of the floor source is the most uniform among the six cases that we considered, followed by the two line sources. There is generally an overall clockwise recirculation in the building; hence the smoke temperature is higher at the left than at the right.

4.2 Predicted smoke flow rates and average temperatures

In Fig. 8, we compare the predicted smoke mass flow rates with the macroscopic analysis results (Gong and Li 2008). The general agreement between the two solutions is very good. The two-way CFD simulations predicted well the existence of the two stable solutions, i.e., the buoyancy-dominated flow solution (in the positive part) and the wind-dominated flow solution (in the negative part). It is noted that the buoyancy-dominated flow solution does not

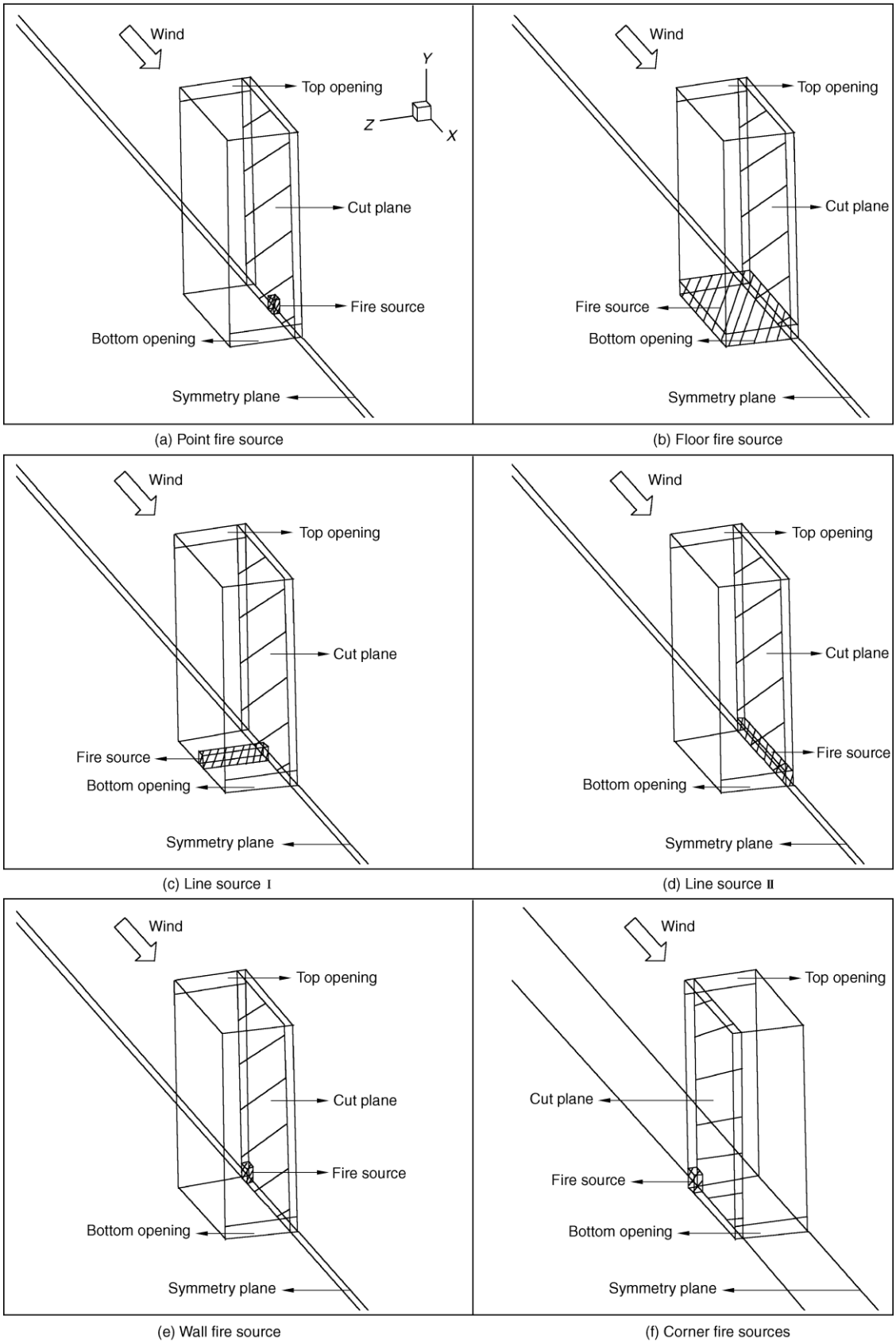

Fig. 5 A summary of the six geometries and locations of fire sources in CFD simulations

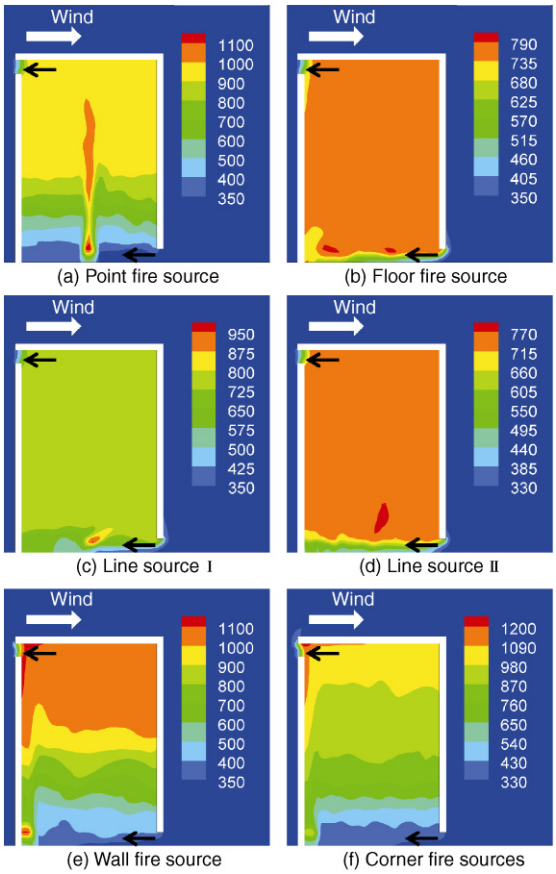

Fig. 6 The predicted temperature (K) contours for the buoyancy-dominated flow solution on the cut plane when the fire power is 32 kW

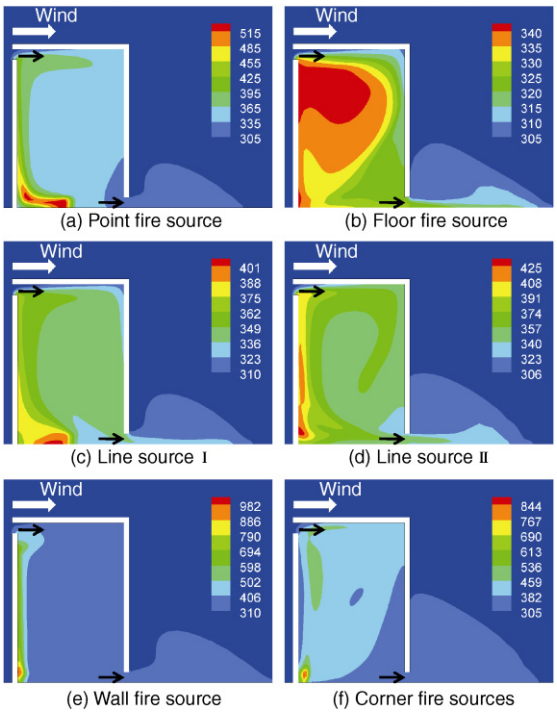

Fig. 7 The predicted temperature (K) contours for the wind-dominated flow solution on the cut plane when the fire power is 32 kW

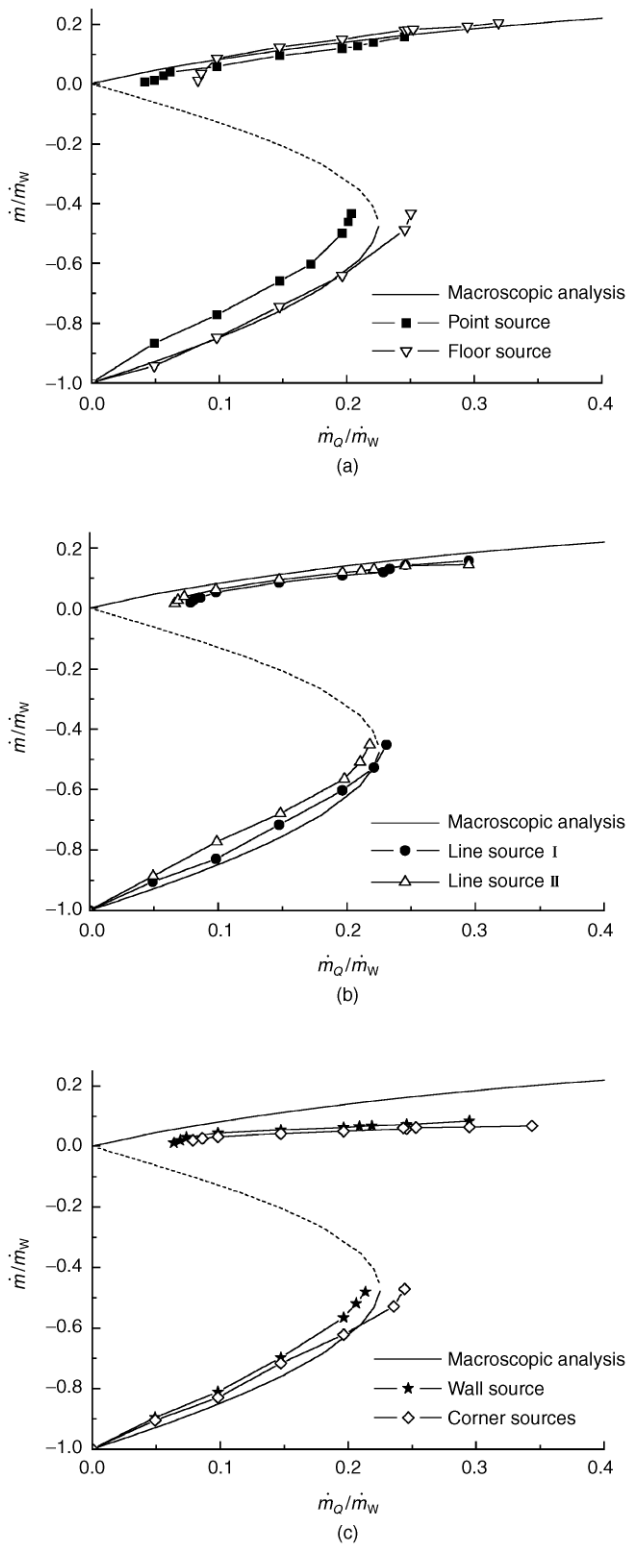

Fig. 8 Comparison of mass flow rate ratios between the macroscopic flow analysis (Gong and Li 2008) and the present CFD simulations when $\dot{m}_Z/\dot{m}_W = 1.5$ and $\dot{m}_A/\dot{m}_W = 1.1$: (a) point and floor sources; (b) line sources I and II; (c) wall and corner sources

exist in the CFD simulations when the ratio $\dot{m}_Q / \dot{m}_W$ is less than a certain threshold of $0.042 - 0.083$ (different values for different cases; see Table 3). The CFD solutions suggest that when the ratio $\dot{m}_Q / \dot{m}_W$ approaches to zero, the buoyancy-dominated flow solution becomes unstable and switches to the wind-dominated flow solution. This solution switching phenomenon was explained in Heiselberg et al. (2004).

It is also interesting to compare the predicted mass flow rates among the six cases. For the buoyancy-dominated flow solution, the CFD predicted flow rate for the floor source is slightly more than the macroscopic value and it gives the largest flow rate when the fire power is identical among the six cases, as shown in Fig. 8. This may be explained that the macroscopic analysis (Gong and Li 2008) assumed a two-layer temperature profile in the building; while in all CFD predictions, the floor source gives the least stratified in all cases. A similar result was observed in natural ventilation (Gladstone and Woods 2001). On the other hand, because the plume attaches to one wall or both walls with reduction of air entrainment, the wall source gives the smaller mass flow rate of smoke and the two corner sources give the smallest. This conclusion is the same as that in the literatures (Zukoski 1995; Poreh and Garrad 2000). For the wind-dominated flow solution, all CFD predicted flow rates are smaller than the macroscopic analysis. The predicted flow rate of the floor source is the greatest among the six cases, closer to the macroscopic value. This may be explained that in our macroscopic analysis a uniform temperature profile in the building is assumed.

It is also useful to examine the averaged smoke temperatures and volume flow rates of smoke through openings in the two stable solutions ($\dot{m}_Q / \dot{m}_W \approx 0.982$, corresponding to a fire power of 32 kW). The results are shown in Tables 1 and 2 respectively.

For the buoyancy-dominated flow, the CFD predicted smoke temperatures are lower than macroscopic analysis for the floor source and two line sources. Perhaps it is due to less thermal stratification in the CFD simulations. CFD predicted smoke flow rates are smaller than the macroscopic analysis for all cases. The floor source resulted in the lowest average temperature and the smallest volume flow rate of exit smoke, while the point source gives the highest average temperature of smoke and the largest volume flow rate of exit smoke.

For the wind-dominated flow, the agreement between the CFD simulations and the macroscopic analysis is relatively better. This is understandable as the uniform assumption in the macroscopic analysis is a rather valid assumption as shown by the CFD results in Fig. 7.

4.3 Predicted critical buoyancy flux ratios

Our key interest is the critical buoyancy flux ratio (at Point 2 in Fig. 4) when the wind-dominated flow switches to the buoyancy-dominated flow. As observed in Fig. 8, the buoyancy-dominated solution also switches to the wind-dominated flow (Point 5 in Fig. 4).

The CFD predicted $\dot{m}_Q / \dot{m}_W$ values at Points 2 and 5 are summarized in Table 3, which is compared well to the

Table 1 The average temperature (K) of smoke at the top opening in the buoyancy-dominated flow solution (buoyancy-top) and at the bottom opening in the wind-dominated flow solution (wind-bottom) when the fire power is 32 kW

Position	CFD						Macroscopic analysis
	Point source	Floor source	Line source Ⅰ	Line source Ⅱ	Wall source	Corner sources	
Buoyancy-top	687.6	526.8	576.4	576.8	683.9	649.7	670.3
Relative deviation (%)	2.58	−21.41	−14.01	−13.95	2.03	−3.07	
Wind-bottom	336.3	331.5	335.0	333.9	335.4	331.9	337.9
Relative deviation (%)	−0.47	−1.89	−0.86	−1.18	−0.74	−1.78	

Table 2 The volumetric flow rate (m^3/s) of smoke through the top opening in the buoyancy-dominated flow solution (buoyancy-top) and through the bottom opening in the wind-dominated flow solution (wind-bottom) when the fire power is 32 kW

Position	CFD						Macroscopic analysis
	Point source	Floor source	Line source Ⅰ	Line source Ⅱ	Wall source	Corner sources	
Buoyancy-top	0.0727	0.0554	0.0596	0.0576	0.0644	0.0559	0.0845
Relative deviation (%)	−13.96	−34.44	−29.47	−31.83	−23.79	−33.85	
Wind-bottom	0.406	0.441	0.441	0.421	0.408	0.429	0.416
Relative deviation (%)	−2.40	6.01	6.01	1.20	−1.92	3.13	

Table 3 The $\dot{m}_Q/\dot{m}_W$ values at the two turning Points 2 and 5 (see Fig. 4), and the $\dot{m}_Q/\dot{m}_W$ difference between Point 5 and Point 2

Point	CFD						Macroscopic analysis
	Point source	Floor source	Line source Ⅰ	Line source Ⅱ	Wall source	Corner sources	
Point 2	0.204	0.250	0.231	0.218	0.213	0.244	0.2241
Point 5	0.042	0.083	0.078	0.066	0.064	0.079	0
Difference	0.162	0.167	0.153	0.152	0.149	0.165	0.2241

macroscopic analysis value. Note that the $\dot{m}_Q/\dot{m}_W$ value of Point 5 cannot be obtained in the macroscopic analysis. The $\dot{m}_Q/\dot{m}_W$ values of both Points 2 and 5 are relatively large for the floor source and relatively small for the point source. The range of the $\dot{m}_Q/\dot{m}_W$ ratio when the solution multiplicity exists is relatively large for the floor source situation.

5 Discussion

The existence of multiple solutions in the simple single-compartment building is not affected by the geometry and location of the fire. The change in the geometry and location of the fire only modifies slightly the smoke temperature and smoke flow rate. However, the smoke flow directions, the smoke temperatures, and the smoke flow rates are very different between the two solutions. For the simple buildings considered here, the smoke flow direction is totally reversed in the two solutions.

Our CFD simulations successfully produced the two different smoke flows under the same fire power and an opposing wind with different initial conditions. The wind-dominated flow with a large fire power was obtained on the basis of previous wind-dominated flow with a small fire power; while the buoyancy-dominated flow with a small fire power was obtained on the basis of previous buoyancy-dominated flow with a large fire power. The two smoke flows can switch to each other when there were sufficient perturbations. For instance, the wind-dominated flow can switch to the buoyancy-dominated flow resorting to increase the fire power over the critical $\dot{m}_Q/\dot{m}_W$ value then reduced the fire power.

The predicted behavior of solution multiplicity of smoke flows is nearly identical to that found in natural ventilation in the same building (Li and Delsante 2001; Li et al. 2001). This is not surprising as the fundamental principles in natural ventilation and the smoke flows are the same apart from the density variation in the smoke flows is much greater and the conventional Boussinesq approximation cannot be used. In theory, smoke flow in building fires is a nonlinear dynamical system in the same way as airflow in natural ventilation, which can exhibit many dynamical characteristics including the solution multiplicity. In the simple building considered here, the multiple solutions are induced by the competing wind and buoyancy forces.

6 Conclusions

The effect of fire source geometry and location on the occurrence of solution multiplicity of smoke flow was studied using CFD simulations in a simple building on fire under an opposing wind. The existence of multiple solutions in the simple single-compartment building was found to be unaffected by the geometry and location of the fire. A zone model is also used to analyze the critical buoyancy flux ratio for the smoke flow multiplicity to exist. The two-way CFD simulations successfully predicted the critical buoyancy flux ratios at the turning Point 2 (Fig. 4). Six fire geometries and locations were simulated. In all six cases, the CFD predicted smoke mass flow rate ratios are in good agreement with the previous macroscopic flow analysis (Gong and Li 2008). A floor source was found to produce the largest smoke flow rate in the buoyancy-dominated flow regime while two corner sources gave the smallest smoke flow rate due to the reduction of air entrainment, and a floor source can have a relatively large smoke flow rate in the wind-dominated flow regime while a point source had a relatively small smoke flow rate. A floor source had a relatively large critical buoyancy flux ratio and the range of fire power to induce smoke flow multiplicity. Our CFD simulations confirmed that different initial conditions can lead to different solutions of smoke flows, and the flow can switch to one another when there are sufficient perturbations.

Acknowledgements

The work described in this paper was supported by a grant from the Seed Funding Programme for Basic Research (Project No. 20062159003) at the University of Hong Kong.

References

Albensoeder S, Kuhlmann HC, Rath HJ (2001). Multiplicity of steady two-dimensional flows in two-sided lid-driven cavities. *Theoretical and Computational Fluid Dynamics*, 14: 223 – 241.

Flynn MR, Caulfield CP (2009). Effect of volumetric heat sources on hysteresis phenomena in natural and mixed-mode ventilation. *Building and Environment*, 44: 216 − 226.

Gladstone C, Woods AW (2001). On buoyancy-driven natural ventilation of a room with a heated floor. *Journal of Fluid Mechanics*, 441: 293 − 314.

Gong J, Li Y (2008). Solution multiplicity of smoke flows in a simple building. In: Proceedings of the Ninth International Symposium on Fire Safety Science, Karlsruhe, Germany, pp. 895 − 906. doi: 10.3801/IAFSS.FSS.9-895.

Heiselberg P, Li Y, Andersen A, Bjerre M, Chen Z (2004). Experimental and CFD evidence of multiple solutions in a naturally ventilated building. *Indoor Air*, 14: 43 − 54.

Heskestad G (1986). Fire plume air entrainment according to two competing assumptions. In: Proceedings of the 21st Symposium on Combustion, Pittsburgh.

Hunt GR, Linden PF (2004). Displacement and mixing ventilation driven by opposing wind and buoyancy. *Journal of Fluid Mechanics*, 527: 27 − 55.

Klote JH, Milke JA (1992). Design of Smoke Management Systems. Atlanta: American Society of Heating, Refrigerating and Air-Conditioning Engineers, Inc.

Lee SL, Emmons HW (1961). A study of natural convection above a line source. *Journal of Fluid Mechanics*, 11: 353 − 368.

Li Y, Delsante A (2001). Natural ventilation induced by combined wind and thermal forces. *Building and Environment*, 36: 59 − 71.

Li Y, Delsante A, Chen Z, Sandberg M, Andersen A, Bjerre M, Heiselberg P (2001). Some examples of solution multiplicity in natural ventilation. *Building and Environment*, 36: 851 − 858.

Li Y, Xu P, Qian H, Deng Q, Wu J (2006). Flow bifurcation due to opposing buoyancy in two vertically connected open cavities. *International Journal of Heat and Mass Transfer*, 49: 3298-3312.

Linden PF, Lane-Serff GF, Smeed DA (1990). Emptying filling boxes: the fluid mechanics of natural ventilation. *Journal of Fluid Mechanics*, 212: 309 − 335.

Linden PF (1999). The fluid mechanics of natural ventilation. *Annual Review Fluid Mechanics*, 31: 201 − 238.

Lishman B, Woods AW (2006). The control of naturally ventilated buildings subject to wind and buoyancy. *Journal of Fluid Mechanics*, 557: 451 − 471.

Lishman B, Woods AW (2009a). On transitions in natural ventilation flow driven by changes in the wind. *Building and Environment*, 44: 666 − 673.

Lishman B, Woods AW (2009b). The effect of gradual changes in wind speed or heat load on natural ventilation in a thermally massive building. *Building and Environment*, 44: 762 − 772.

McCaffrey BJ (1979). Purely Buoyant Diffusion Flames: Some Experimental Results. NBSIR 79-1910, National Bureau of Standards.

Morton BR, Taylor G, Turner JS (1956). Turbulent gravitational convection from maintained and instantaneous sources. In: Proceedings of the Royal Society of London, A234: 1 − 23.

National Fire Protection Association (NFPA) (2009). NFPA 92B: Standard for smoke management systems in malls, atria and large spaces. Quincy, MA: NFPA.

Nitta K (1999). Variety modes and chaos in smoke ventilation by ceiling chamber system. In: Proceedings of the Sixth International IBPSA Conference, Kyoto, Japan, pp. 473 − 480.

Nitta K (2001). Variety modes and chaos in natural ventilation or smoke venting system. In: Proceedings of the Seventh International IBPSA Conference, Rio de Janeiro, Brazil, pp. 635 − 642.

Poreh M, Garrad G (2000). A study of wall and corner fire plumes. *Fire Safety Journal*, 34: 81 − 98.

Strogatz SH (1994). Nonlinear Dynamics and Chaos—with Applications to Physics, Biology, Chemistry, and Engineering. Reading: Addison-Wesley.

Yuan J, Glicksman LR (2007). Transitions between the multiple steady states in a natural ventilation system with combined buoyancy and wind driven flows. *Building and Environment*, 42: 3500 − 3516.

Yuan J, Glicksman LR (2008). Multiple steady states in combined buoyancy and wind driven natural ventilation: The conditions for multiple solutions and the critical point for initial conditions. *Building and Environment*, 43: 62 − 69.

Yuan LM, Cox G (1996). An experimental study of some line fires. *Fire Safety Journal*, 27: 123 − 139.

Zukoski EE, Kubota T, Cetegen B (1980). Entrainment in fire plumes. *Fire Safety Journal*, 3: 107 − 121.

Zukoski EE (1995). Properties of fire plume. In: Cox G (ed), Combustion Fundamental of Fire (pp. 101 − 220). London: Academic Press.